Wave Excitation Tests on a Fixed Sphere: Comparison of Physical Wave Basin Setups

Jacob Andersen and Morten Bech Kramer

Abstract— **Wave excitation tests on a fixed sphere with the center at the still water level were carried out with three different physical wave basin setups. The tests were completed as a continued effort of the working group OES Wave Energy Converters Modelling Verification and Validation to increase confidence in numerical models of wave energy converters by generation of accurate benchmarks datasets for numerical model validation. An idealized testcase with wave excitation of a fixed sphere to be used with the benchmarks was formulated. The three investigated physical wave basin setups included: 1) a six degree-of-freedom load cell mounted to the top of the sphere, 2) a bending beam force transducer mounted to the top of the sphere, and 3) a system of six pretensioned wires mounted to the top and bottom of the sphere with force transducers attached to each wire. The aim of the present paper is to identify the best representation of the idealized testcase. To this end, the three experimental setups are inter-compared in terms of dynamic properties, sensitivity, and disturbances of the water phase from the presence of measurement equipment. Low inter-experiment variability was disclosed, i.e., 5-8% depending on wave-nonlinearity, indicating accurate representations of the idealized testcase across all setups. Setup 3 was found to be the more accurate representation and further work with this setup to release a public benchmark dataset was planned.**

Keywords— **physical tests, benchmark dataset, sphere, wave excitation force, WEC, fluid–structure interaction.**

I. Introduction

DESIGN of wave energy converters (WECs) relies on accurate numerical modelling of fluid-structure interaction problems. Prior to the practical usage of numerical models, validation exercises are critical to ensure proper accuracy of the numerical model in conditions representative of the intended model use. The uncertainty of the validation benchmark dictates the lower bound of uncertainty ascribed to the numerical model from validation and in the case of benchmarking of numerical models from accuracy whether distinctions can be made with a given confidence level. Accordingly, low-uncertainty benchmarks are key in developing accurate numerical models which ultimately can drive lower design costs of WECs as less conservative design values can be attained.

Experiments dedicated to generating highly accurate benchmark datasets for numerical modelling of WECs were developed under the OES Wave Energy Converters Modelling Verification and Validation (formerly, OES
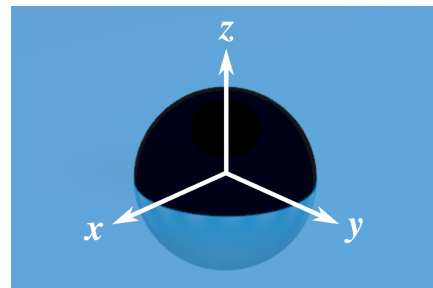

Fig. 1. Sphere under still water conditions with global Cartesian coordinate system (origin at sphere geometrical center).

Task 10) working group and published in [1] with heave decay tests on a floating sphere submerged to the equator. The dataset was showcased by benchmarking numerical models of various fidelity against it and the value of having low uncertainty bounds on the benchmarks was demonstrated. Resultantly, the OES working group decided to extent the work to comprise accurate benchmark datasets on wave excitation tests. To this end, physical wave basin tests were designed and carried out at the Ocean and Coastal Engineering Laboratory of Aalborg University, Denmark, and based on these an idealized testcase on wave excitation of a fixed sphere was formulated, see Section I-A. The idealized testcase is introduced to allow for simple, yet accurate, representation of the physical tests underlying the benchmark dataset in numerical models (as in [1]). Consequently, the physical parameters of the idealized testcase are derived from the physical tests. Idealized
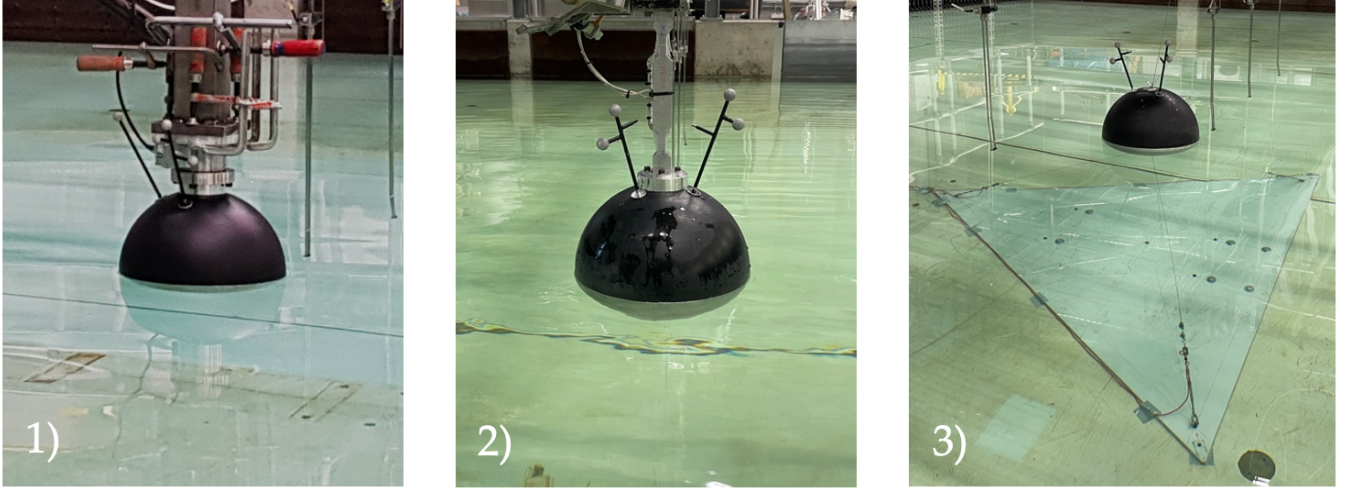
Fig. 2. Investigated experimental setups: 1) six-DoF load cell, 2) bending beam force transducer (2-DoF), and 3) system of six pretensioned wires with one-DoF force transducers.

assumptions are introduced to obtain a simple testcase intuitively adopted for validation exercises by others. The sphere tests are altogether completed as Phase V of the work by the OES working group and are referred to as the *Kramer Sphere Cases*.

A. The Idealized Testcase

Consider a rigid sphere of radius $r = 150$ mm fixed at the interface between an air and a water phase. A global Cartesian coordinate system is defined with the origin at the geometrical center of the sphere, the xy-plane at the still water level (SWL), and z positively oriented upwards, see Fig. 1. The air phase is unbounded whereas the water phase is bounded by a solid, horizontal bed at $z = -h$.

TABLE I
WAVE CONDITIONS

Case	H (m)	T (s)	$H/(2r)$ (-)	η_{crest}/r (-)	η_{trough}/r (-)	H/L (%)
R01	0.0181	1.14	0.06	0.06	-0.06	0.9
R02	0.0193	0.72	0.06	0.07	-0.06	2.4
R03	0.0182	0.51	0.06	0.06	-0.06	4.4
R04	0.0560	1.25	0.19	0.19	-0.18	2.3
R05	0.0561	0.88	0.19	0.20	-0.17	4.5
R06	0.0512	0.62	0.17	0.19	-0.15	8.0
R07	0.1496	2.65	0.50	0.57	-0.43	2.1
R08	0.1463	1.58	0.49	0.53	-0.44	4.0
R09	0.1534	1.08	0.51	0.58	-0.44	7.9
R10	0.2776	4.18	0.93	1.35	-0.51	2.2
R11	0.2459	2.28	0.82	0.98	-0.66	4.0
R12	0.2611	1.42	0.87	1.02	-0.72	8.1

The sphere is subjected to long-crested, incident, regular waves propagating in positive x. 12 regular wave conditions (prefix R) of low to high nonlinearity are given in Table I where H and T denotes wave height and wave period, respectively. The wave steepness H/L and ratio of crest elevation to sphere radius η_{crest}/r as well as trough elevation to sphere radius η_{trough}/r are calculated by stream function theory as per [2]. Please note that the crest

elevations of the R10 and R12 waves are larger than r signifying large wave-overtopping effects in these conditions. $\rho_{water} = 998.2$ kg/m³ is the density of the water phase and $g = 9.82$ m/s² is the acceleration due to gravity.

B. Scope of the Paper

Three physical wave basin setups were tested to investigate the most accurate representation of a sphere fixed with the center at SWL, i.e., without any support structure, as per the idealized testcase. The experimental setups were all aimed at high rigidity to mimic the fixation from the idealized testcase while maintaining good sensitivity and low disturbances of the force measurement equipment. The three experimental setups included 1) A traditional six degrees of freedom (six-DoF) load cell mounted to the top of the sphere, 2) A bending beam force transducer with two full Wheatstone bridges (two-DoF), 3) A system of six pretensioned wires with a one-DoF force transducer attached to each, see Fig. 2. All setups utilized the CNC machined physical sphere model from the decay tests in [1]. The focus points in the development of the setups were:

- *Rigidity*. Focus was to ensure a highly rigid support of the sphere in order to reduce the influence of dynamic amplification on the measured wave forces.
- *Sensitivity*. The force measurement equipment should have good sensitivity over the tested range of wave conditions.
- *Disturbances*. The influence of the presence of the measurement equipment on the measured wave forces on the sphere should be marginal.

The aim of the present paper is to assess the accuracy of the three experimental setups to represent the idealized testcase. Since no highly accurate benchmark of the testcase is available (the ultimate objective is exactly that) the assessment will be based on inter-experiment
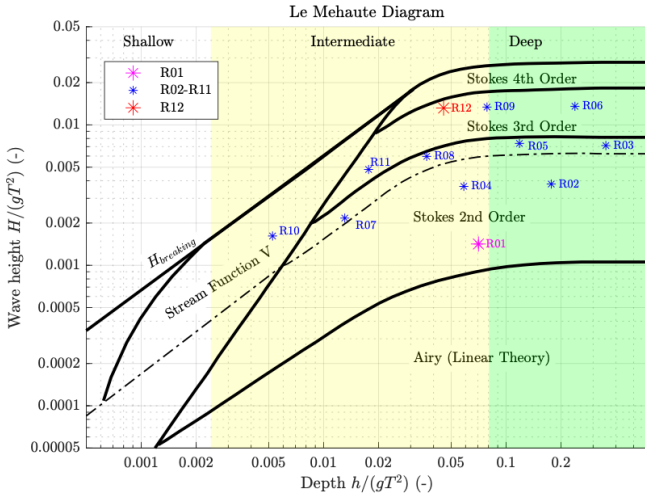
Fig. 3. Wave conditions (Table I) with boundaries from [3].

comparisons with emphasis on modal parameters (rigidity), deformation of the free surface around the sphere from video recordings (disturbances), and time series of the wave excitation force (disturbances, sensitivity). In the present paper the horizontal and vertical wave excitation forces F_x and F_z are considered, although F_x is the sole force measurement extracted in Setup 2. However, if Setup 2 turns out to be the more appropriate, the bending beam force transducer can be oriented to measure F_z in additional tests.

The regular wave conditions included in the idealized testcase Table I are visualized in Le Mehauté's diagram [3] in Fig. 3 where the wave conditions with the highest and lowest steepness are highlighted, i.e., *R12* and *R01*, respectively. These two wave conditions are used as the basis for the assessment of the suitability of the experimental setups to represent the testcase due to brevity and as these constitute the upper and lower bounds of wave height and nonlinearity.

II. Experimental Setups

All experimental setups used the sphere model from the heave decay tests of [1], see Fig. 4. Two hemispheres were CNC machined out of aluminum blocks with an accuracy of 0.1 mm. As seen in Fig. 2 the model has two M8 threaded holes, one in the top and one in the bottom. The
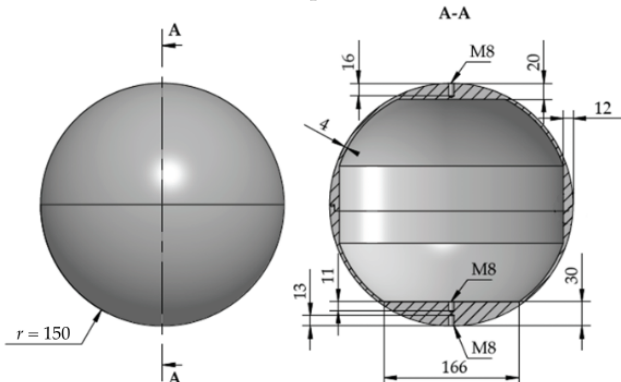

Fig. 4. Technical drawing of the sphere. Measurements in mm. Refer to [1] for further details.

two holes allows for attachment of force measurement equipment. The sphere model is described in detail in [1]. The tests were carried out at the wave basin in the Ocean and Coastal Engineering Laboratory of Aalborg University, Denmark. The wave basin was equipped with piston-type wavemakers and vertical passive absorption. The active area of the wave basin measured 8.44 m (mean piston position to passive absorption) times 13.00 m (between side walls) with the sphere installed at the center. Separate tests without the sphere model were carried out with a wave gauge installed at the position of the sphere model in order to align force time series to incident waves. Waves were generated by second order or approximate stream function wavemaker theory as per [4] and [5], respectively, in accordance with Fig. 3. Identical steering signals were used between tests of same wave condition. Reflective markers were mounted to the top of the sphere model to measure vibrations by an optical motion tracker system. Furthermore, three arrays of wave gauges were installed around the sphere. The motion tracker system and the wave gauge arrays were included for further analyses to be published with the benchmark datasets and are beyond the scope of the present paper.

C. Setup 1 (six-DoF load cell)

A six-DoF load cell, capable of measuring force/moment in three dimensions, was connected to the top of the sphere model via transition pieces in Setup 1, see Fig. 5. The lower transition piece was a solid steel cylinder of 900 mm in diameter with a convex spherical curvature at the bottom
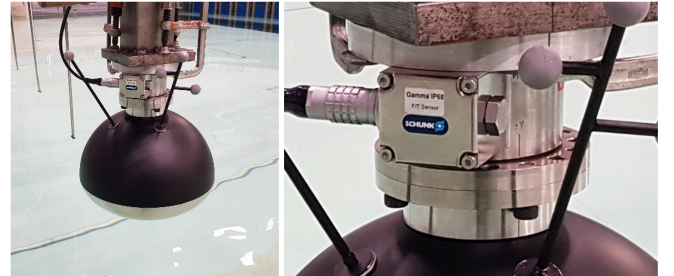

Fig. 5. Close-up of six-DoF load cell in Setup 1.

face of radius 150 mm (fitting the sphere surface) installed for proper load transfer from the sphere model. The upper transition pieces were two steel cylinders of 115 mm in diameter needed for assembly of the load cell. A steel beam mounted to the wave basin bridge was the support of the setup. The load cell was an ATI Industrial Automation Gamma IP68 SI-65-5 with a force measurement range on F_x of 65 N and a resolution of 1/80 N. A calibration certification was provided by the producer ATI declaring the uncertainty of the measured F_x with a semi-interval of 0.75% of the full-scale load, i.e., 0.49 N, at the 95% confidence level. However, tests with precision weights in a truss system to generate accurate F_x excitation indicated that the uncertainty was significantly (about an order of magnitude) lower for F_x at the (relatively low) load levels imposed with the testcase.

D. Setup 2 (bending beam force transducer)

A force transducer with two full Wheatstone bridges to measure bending about the y-axis was mounted through a transition piece to the top of the sphere, see Fig. 6. The internal moments about y at the two bridges were used to
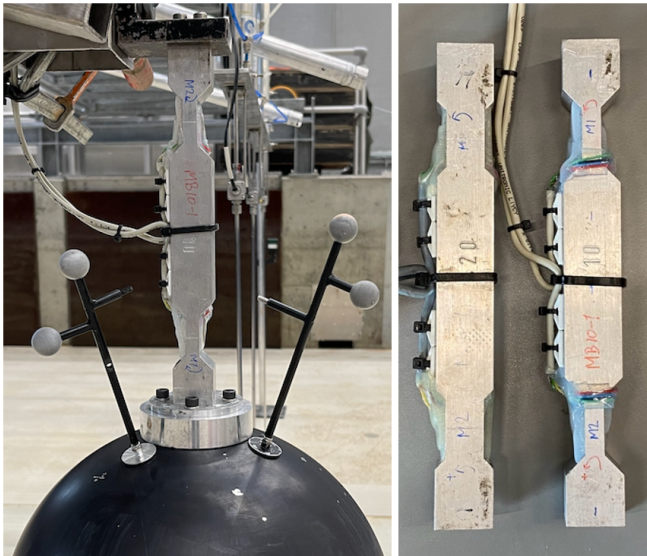

Fig. 6. Close-up of force transducer in Setup 2a (left) and force transducers from Setups 2a and 2b (right).

calculate the resulting force F_x (and its point of attack). Two force transducers were employed with thicknesses at the bridge positions of 10 mm and 20 mm (henceforth referred to as Setup 2a and 2b, respectively) to vary the stiffness of the transducers, see Fig. 6. The transition piece is identical to the lower transition piece of Setup 1, i.e., 900 mm in diameter. The force transducers were made of aluminum and had an inter-bridge distance of 150 mm. With a linear calibration function, the force transducers were calibrated against nine known moments from precision weights supported with different arms.

E. Setup 3 (system of pretensioned wires)

Six wires were pretensioned between the sphere model and two solid triangular steel plates of 10 mm thickness, see Fig. 7. The wires were attached to a M8 steel eyelet lowered into the sphere model at the top and bottom reducing the impact with overtopping waves. The plates
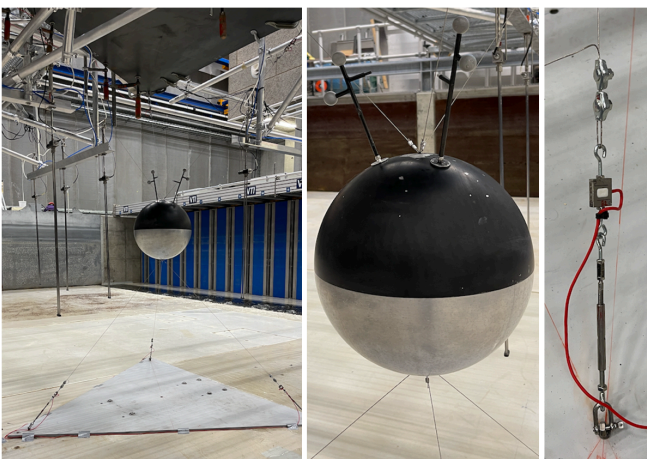

Fig. 7. Setup 3 with close-up of attachment of pretensioned wires (center) and one-DoF force transducer (right).

were clamped to the wave basin bridge or bolted to the bed, respectively. A one-DoF force transducer was assembled to each wire allowing the calculation of forces in three dimensions and moments about x and y given the direction vector of each wire. The direction vectors were derived from meticulous measurement of the coordinates of the fixation points on the sphere model and the triangular support plates. FUTEK LSB210 one-DoF force transducers were utilized which had a range of 450 N. The wires had a diameter of 1 mm and were pretensioned to about 300 N estimated to allow for the maximum tensions from the wave loads while not exceeding the range of the one-DoF force transducers. The one-DoF transducers were calibrated against known forces from precision weights with 10-point linear calibration over a range of 0 to 450 N.

III. DYNAMIC AMPLIFICATION

The modal parameters of the three setups were calculated from force decay time series after excitation of the sphere model with an impulse-like load, see example in Fig. 8. Calculation of modal parameters were limited to the damped eigenfrequency f_{ed} and damping ratio ζ in x in the present paper (stiffness in z of Setups 1 and 2 were very high). The modal parameters of the three setups were calculated with the software package WaveLab 3.877 [6] and are given in Table II.

Based on the modal parameters, corrections to the dynamic amplification were calculated under the assumption of a linear, one-DoF mass-spring-damper-system as per [7], yielding a dynamic amplification filter with gain (inverse dynamic amplification factor) and
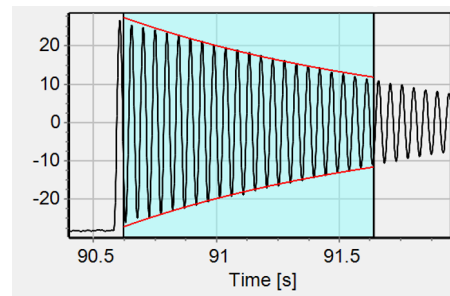

Fig. 8. Force decay time series from Setup 3 used for modal analysis with WaveLab [6]. The y-axis indicate force [N].

TABLE II
MODAL PARAMETERS AND COMPENSATION METRICS

Setup	f_{ed} (Hz)	ζ (-)	$\beta_{c,R01}$ (%)	$\beta_{c,R12}$ (%)	$\beta_{rc,R01}$ (%)	$\beta_{rc,R12}$ (%)
1	20.0	0.026	10.9	5.7	688	142
2a	7.4	0.009	2.8	12.7	181	322
2b	12.9	0.007	1.5	5.4	100	136
3	20.9	0.006	2.2	3.9	152	100

phase (inverse phase) for the three setups as shown in Fig. 9. The gain should ideally be unity indicating no compensation is required. The frequencies of the wave conditions in the idealized testcase are in the range 0.24 to 1.96 Hz which yields gains of minimally 93% in Setup 2a and above 99% for the Setups 1, 2b, and 3 indicating only
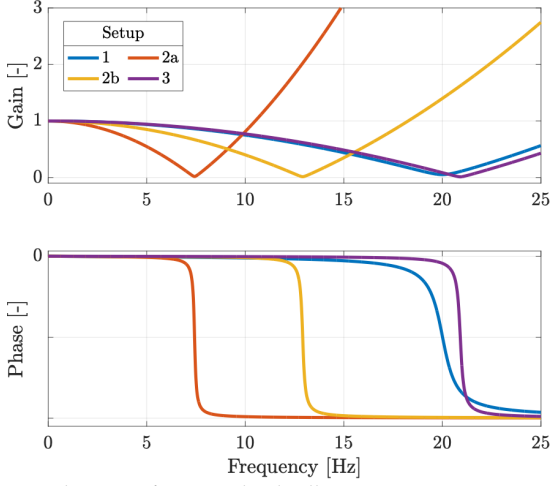
Fig. 9. Close-up of six-DoF load cell in Setup 1.

very little dynamic amplification from the main wave frequency for all setups but Setup 2a which may be questionable to use over the full range of wave conditions especially without compensation measures. The gain is close to zero around the respective eigenfrequencies which together with the damping ratios of Table II signify how the setups are lightly damped. This underlines the importance of having high eigenfrequencies relative to the wave frequencies to reduce inaccuracies from the compensation as much as possible.

The influence of the dynamic amplification filter on the force time series was quantified by a compensation metric β_c which is the standard deviation of the difference between the filtered and unfiltered force time series, i.e.,

$$\beta_c = \frac{\text{std}\left(F_{x,UF}(t) - F_{x,F}(t)\right)}{\text{std}\left(F_{x,F}(t)\right)} \qquad (1)$$

where std is the standard deviation, t is time, and subscripts UF and F refer to the unfiltered and filtered signals, respectively. β_c was calculated for the three setups employing the dynamic amplification filter with a low-pass cut-off frequency of 25 Hz to the force time series of a single wave (as extracted in Section V) in wave conditions $R01$ and $R12$, see Table II. β_{rc} is introduced in Table II as the relative compensation metric with the lowest β_c value as reference. Examples of the influence of the dynamic amplification filtering on the measured force time series of the extracted single waves (as explained in Section V) with close-ups are shown for $R01$ and $R12$ in Fig. 10. Forces are normalized with the buoyancy of the sphere at initialization F_{b0} (stagnant water).

The dynamic amplification compensation by β_c, see (1), is in general lower in wave condition $R01$ relative to $R12$ where the larger wave heights and nonlinearity cause larger, more rapid impacts with the setups. The force time series of Setup 1 are compensated the most in $R01$, as also shown in Fig. 10. Despite the eigenfrequencies of Setups 1 and 3 being of approximately equal size, the compensation from dynamic amplification is increased 42% for Setup 1. This may be an effect of the slamming-like loads on the load cell and transition pieces in Setup 1 (as in Setups 2a and 2b) during overtopping of the $R12$ wave which are not present for Setup 3. The highest compensation in $R12$ is seen for Setup 2a which has the same projected area to the yz-plane as Setup 2b but has significantly reduced stiffness.

IV.   DISTURBANCES FROM MEASUREMENT EQUIPMENT

Snapshots are extracted from video recordings (framerate of 30 Hz) for all setups at the time coordinate corresponding to the second wave crest after ramp-up have propagated to the center of the sphere, see Fig. 11. Clearly, the wave overtopping is accelerated differently between the three setups due to the presence of the measurement equipment. Setup 1 seems to better guide the overtopped water around the load cell relative to Setup 2 which yields the highest (visible) run-up – presumably due to the cylindrical and rectangular cross-sections of the measurement equipment in Setups 1 and 2, respectively. The wave smoothly overtopped the sphere model in Setup 3 where no acceleration of the water phase
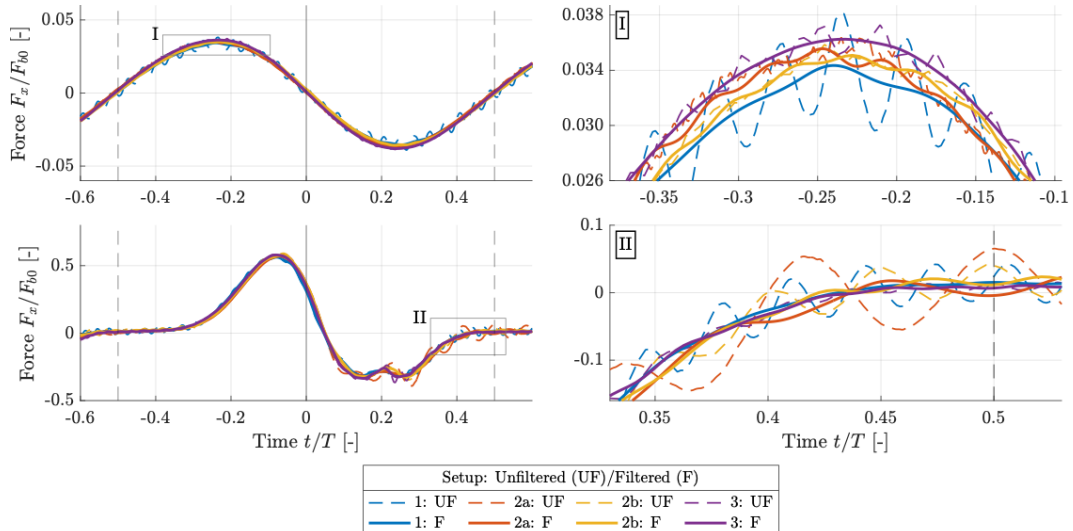

Fig. 10. Influence of dynamic amplification filter on force time series in $R01$ (upper) and $R12$ (lower).
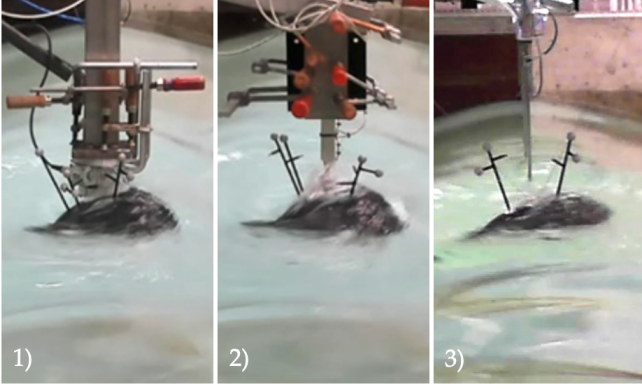
Fig. 11. Wave-overtopping in *R12* for Setups 1-3.

Fig. 12. Incident waves and ring wave at the sphere model in in *R12* for Setup 3 without reflective markers.

Fig. 13. Projected areas to the *yz*-plane for Setups 1-3. Identical scaling between setups.

from the wires were detected. The snapshots reveal how most of the downwave side of the top hemisphere is exposed due to the formation of an outward propagating ring wave. The ring wave are shown with a smooth incident wave field in Fig. 12 for the same time coordinate as Fig. 11. The minimal interaction between overtopping and measurement equipment in Setup 3 suggests an undisturbed overtopping of the sphere (as idealized in the testcase) of about 50 mm (estimated from video recordings). Despite the small visual intrusion on wave overtopping from the wires in Setup 3, the projected area of the wires and sphere model to the *yz*-plane (as seen from the wavemaker) is similar to that of Setup 2. Introducing A_{ref} as the projected area to the *yz*-plane of the idealized testcase, i.e., a circle of radius $r = 150$ mm, the relative increase in the projected area for each setup is calculated in (2).

$$\gamma_A = (A_i - A_{ref})/A_{ref} \qquad (2)$$

where A_i is the projected area to the *yz*-plane of the setups (sphere model, measurement equipment, transition pieces, etc.) between $z = -h$ and $z = z_{ot}$ where z_{ot} is the maximum elevation of overtopping detected in Setup 3, i.e., with the least interference from measurement equipment, which was estimated as $z_{ot} = 200$ mm. The relative increases of the projected areas γ_A are then 7.2%, 4.0%, and 3.7% for Setups 1-3, respectively. Accordingly, the increase of the projected area relative to the idealized testcase is about double in Setup 1 relative to Setup 3 (and 1.8 relative to Setup 2) whereas Setups 2 and 3 varies with less than 10%. It should however be noted that most waves included in the idealized testcase (and indeed wave conditions *R01* and *R12*) are in the deep-water wave regime, as shown in Fig. 3, and particle velocities consequently increases 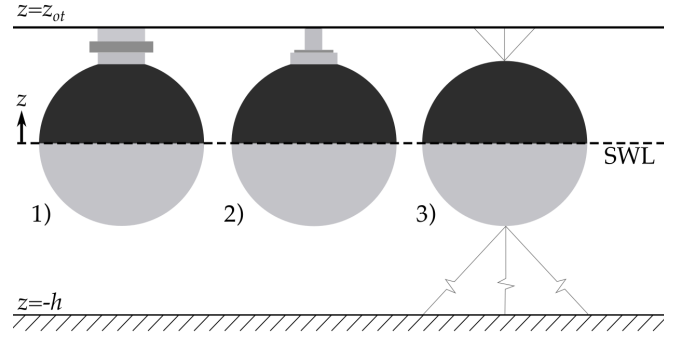exponentially from the bed to the free surface yielding only minor wave forces on the parts of the wires close to the bed. The major differences in the projected area in the vicinity of the free surface and the sphere model from the three setups can be appreciated in Fig. 13 where projected *yz*-plane views of the setups are identically scaled.

V. WAVE EXCITATION FORCES

Surface elevation time series from the tests with a wave gauge installed at the position of the center of the sphere model (without the sphere model) were used to extract a window of the F_x and F_z force time series corresponding to the first full wave after transient effects in the wave signal from, e.g., wave-ramp-up, were assessed to be sufficiently low, see Figs. 14-17. Close-ups on the extracted waves with additional close-ups on the force extrema are given in Figs. 15 and 17. The surface elevation time series and wave excitation force time series of each setup are aligned from trigger signals.

The close-ups on the extracted waves show virtually overlapping F_x and F_z time series for all setups in both *R01* and *R12*. It should be noted that F_z is only measured in Setups 1 and 3. The additional close-ups around force extrema show somewhat minor deviations between the force time series with the generally largest deviations between Setup 1 and 3. The relative deviations in force extrema and standard deviation (global value) of the extracted waves are denoted δ and are given in Table III with the minimum absolute value as reference and subscripts *min*, *max*, and *std* indicating minima, maxima, and standard deviation, respectively. The relative deviations are highest for *R01* relative to *R12* presumably due to the lower loads of *R01* yielding relatively larger impacts from offset-type uncertainties in the force measurement process with the setups (rather than the force transducers themselves which calibration uncertainties are significantly smaller). This is supported by the nearly constant offsets between force time series around force extrema for *R01* in Fig. 15 and is further indicated from the nearly constant deviations of F_x within each setup in wave condition *R01*, i.e., 1-2% for Setup 2a, 2-3% for Setup 2b, 6-8% for Setup 3 relative to Setup 1, see Table III. In wave condition *R12*, the force time series around force extrema and the relative deviations vary more as shown in Fig. 17 and Table III indicating not only
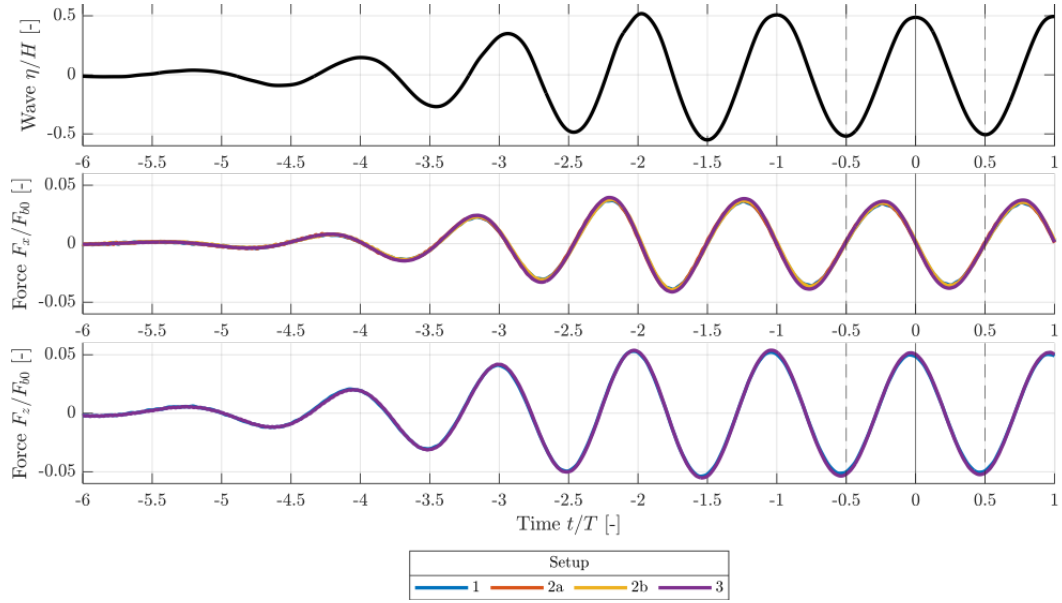
Fig. 14. Surface elevation and force time series with extraction of wave in *R01*. η/H adheres to tests without sphere model.
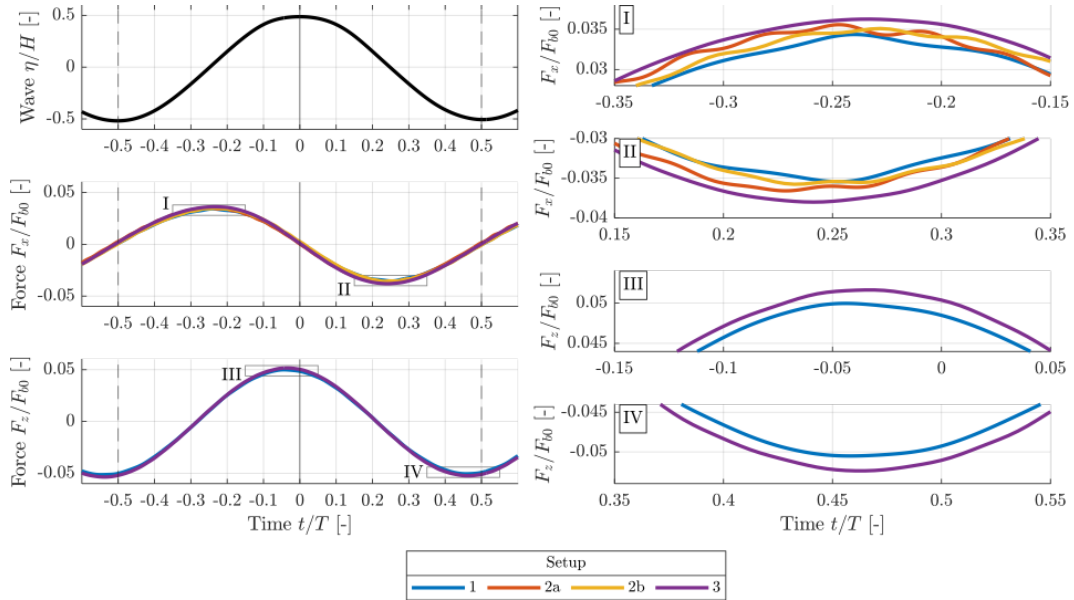

Fig. 15. Surface elevation and force time series of extracted wave with close-ups on force extrema in *R01*.

measurement uncertainties but differences in the experienced hydrodynamics between setups such as the detected different interactions between overtopping waves and measurement equipment. That being said, the relative deviations are in general low with deviations less than 8% in *R01* and less than 5% for *R12* for all setups. The high consistency of the measured force time series substantiates that all experimental setups are capable of accurately capturing the wave excitation forces on a fixed sphere as per the idealized testcase. Small oscillations in x were present in Setups 2a and 2b after dynamic amplification filtering as can be seen in Fig. 15. Furthermore, small oscillations are present in z for Setup 1 in *R12*, see Fig. 17, which gives a slight edge to Setup 3 – the only other setup measuring both F_x and F_z. The large deviation of Setup 3 relative to Setup 1 at about $t/T = -1$ in the F_z time series of wave condition *R12* occurs at the impact of the high, leading wave after ramp-up to the load cell, see Fig. 16.

TABLE III
RELATIVE DEVIATIONS OF FORCE EXTREMA AND STANDARD DEVIATIONS BETWEEN SETUPS (REFERENCE TO THE MINIMUM ABSOLUTE VALUE).

			R01			
Setup	$\delta_{min,x}$ (%)	$\delta_{max,x}$ (%)	$\delta_{std,x}$ (%)	$\delta_{min,z}$ (%)	$\delta_{max,z}$ (%)	$\delta_{std,z}$ (%)
1	0.0	0.0	0.0	0.0	0.0	0.0
2a	3.3	3.5	3.7	-	-	-
2b	0.9	2.1	2.3	-	-	-
3	7.3	5.5	8.0	3.7	3.3	3.7

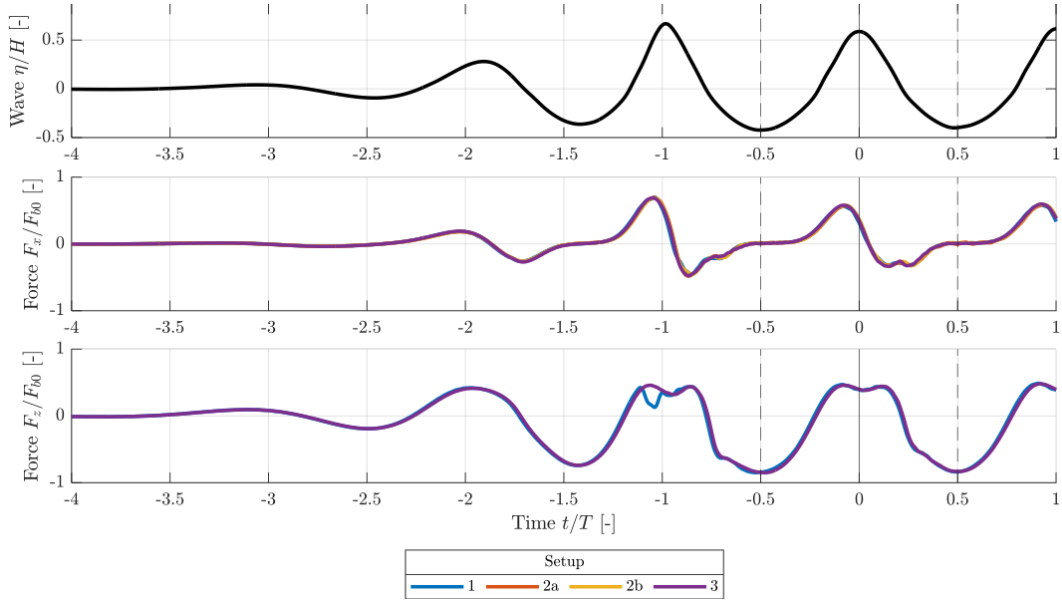|			*R12*			
Setup	$\delta_{min,x}$ (%)	$\delta_{max,x}$ (%)	$\delta_{std,x}$ (%)	$\delta_{min,z}$ (%)	$\delta_{max,z}$ (%)	$\delta_{std,z}$ (%)
1	0.0	0.0	0.0	0.0	2.4	0.0
2a	0.5	1.3	1.2	-	-	-
2b	1.7	2.5	1.4	-	-	-
3	4.7	2.9	2.4	1.0	0.0	0.9

Fig. 16. Surface elevation and force time series with extraction of wave in *R12*. η/H adheres to tests without sphere model.
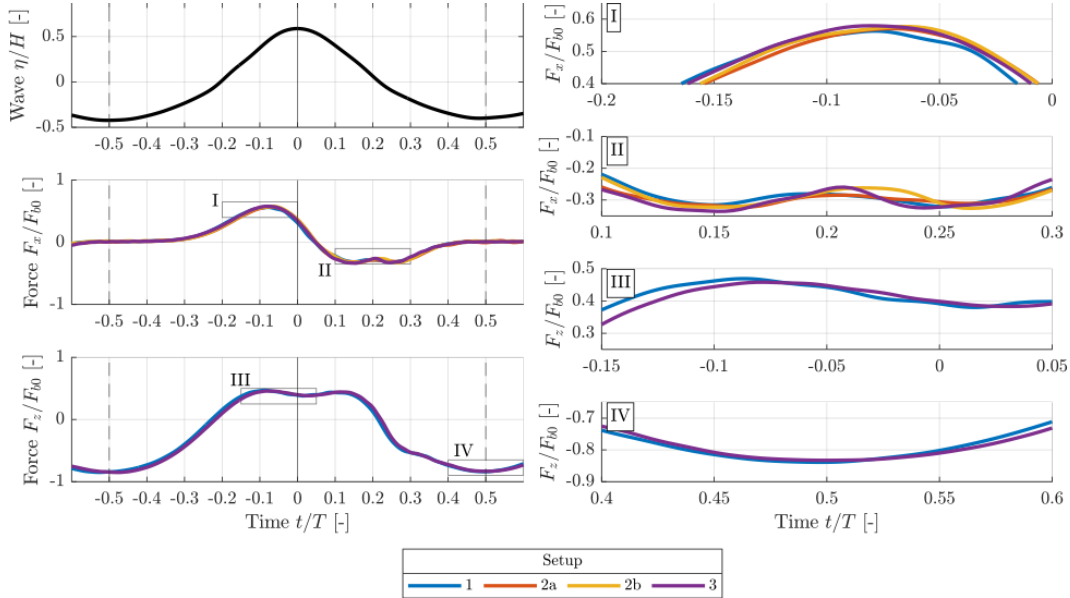

Fig. 17. Surface elevation and force time series of extracted wave with close-ups on force extrema in *R12*.

VI. CONCLUSIONS AND FURTHER WORK

The accuracy of three physical wave basin setups to represent an idealized testcase on wave excitation of a fixed sphere with the center at the SWL was investigated. Setup 3 (system of pretensioned wires) was the most rigid setup with the least corrections due to dynamic amplification for the investigated wave conditions, i.e., *R01* and *R12* (extrema of wave heights and steepness included in the testcase). Setup 3 further had the least interference with overtopping waves (estimated from video recordings) and the least projected area normal to the wave propagation direction – especially if weighting with the intermediate- to deep-water velocity profiles of the incident waves. Wave excitation force time series were extracted for F_x for all setups whereas F_z was only measured in Setups 1 and 3. Low inter-experiment variability on wave excitation force time series were found across all setups, i.e., maximally 8% and 5% deviation on force extrema and standard deviation for *R01* and *R12*,

respectively. The deviations of the wave excitation force between setups in the close to linear wave condition *R01* were ascribed to measurement uncertainties while in the higher, nonlinear wave condition *R12* the deviations were ascribed to both measurement uncertainties and differences in the disturbances from measurement equipment to the wave field due to wave-overtopping. Accordingly, Setup 3 is assessed to be the more accurate representation of the idealized testcase from the investigated range of setups. However, the low inter-experiment variability on the measured wave excitation force time series (after dynamic amplification filtering) indicates how all the experimental setups accurately represent the idealized testcase with relatively small implications from the detected differences in dynamic properties and disturbances from measurement equipment on the wave excitation forces.

Further work with Setup 3 is currently undertaken including quantification of uncertainty of the force measurement process. Two testcases with, respectively, an

idealized [8] and a physical/detailed [9] representation of the physical tests were made public to encourage numerical modelling of the testcase. Results based on Setup 3 are planned to be released as a public benchmark dataset with confidence bounds and comparison to numerical models of various fidelity.

REFERENCES

[1]   M. B. Kramer *et al.*, "Highly accurate experimental heave decay tests with a floating sphere: A public benchmark dataset for model validation of fluid–structure interaction," *Energies (Basel)*, vol. 14, no. 2, Jan. 2021, doi: 10.3390/en14020269.

[2]   J. D. Fenton, "The Numerical Solution of Steady Water Wave Problems," *Comput Geosci*, vol. 14, no. 3, pp. 357–368, Jan. 1988, doi: 10.1016/0098-3004(88)90066-0.

[3]   B. Le Méhauté, "An Introduction to Water Waves," in *An Introduction to Hydrodynamics and Water Waves*, Berlin, Heidelberg: Springer Berlin Heidelberg, 1976, pp. 197–211. doi: 10.1007/978-3-642-85567-2_15.

[4]   H. A. Schäffer, "Second-Order Wavemaker Theory for Irregular Waves," *Ocean Engineering*, vol. 23, no. 1, pp. 47–88, 1996, doi: https://doi.org/10.1016/0029-8018(95)00013-B.

[5]   H. Zhang and H. A. Schäffer, "Approximate Stream Function Wavemaker Theory for Highly Non-Linear Waves in Wave Flumes," *Ocean Engineering*, vol. 34, no. 8, pp. 1290–1302, 2007, doi: https://doi.org/10.1016/j.oceaneng.2006.04.010.

[6]   P. Frigaard and T. L. Andersen, *Analysis of Waves: Technical Documentation for WaveLab 3*, no. 33. in DCE Lecture notes. Denmark: Department of Civil Engineering, Aalborg University, 2014.

[7]   S. R. K. Nielsen, *Vibration Theory, Vol. 1: Linear Vibration Theory*, 3rd edition. in U/. Denmark: Department of Civil Engineering, Aalborg University, 2004.

[8]   M. B. Kramer, J. Andersen, and K. Nielsen, *Wave Excitation Forces on a Sphere: Description of an Idealized Testcase*, 1st ed., no. 307. in DCE Technical Reports. Department of the Built Environment, Aalborg University, 2023.

[9]   M. B. Kramer and J. Andersen, *Wave Excitation Forces on a Sphere: Description of a Physical Testcase*, 1st ed., no. 307X. in DCE Technical Reports. Department of the Built Environment, Aalborg University, 2023.